Temperature-induced Lifshitz transition and possible excitonic instability in ZrSiSe

F. C. Chen,[1,2,*] Y. Fei,[3,*] S. J. Li,[4,5,6,*] Q. Wang,[5,2] X. Luo,[1,†] J. Yan,[1,2] W. J. Lu,[1] P. Tong,[1] W. H. Song,[1] X. B. Zhu,[1] L. Zhang,[5] H. B. Zhou,[5] F. W. Zheng,[4] P. Zhang,[4,7] A. L. Lichtenstein,[8,9] M. I. Katsnelson,[9,10] Y. Yin,[3,11,‡] Ning Hao,[5,§] and Y. P. Sun[5,1,11,¶]

[1]*Key Laboratory of Materials Physics, Institute of Solid State Physics, HFIPS, Chinese Academy of Sciences, Hefei, 230031, China*
[2]*University of Science and Technology of China, Hefei, 230026, China*
[3]*Department of Physics, Zhejiang University, Hangzhou, 310027, China*
[4]*Institute of Applied Physics and Computational Mathematics, Beijing, 100088, China*
[5]*Anhui Province Key Laboratory of Condensed Matter Physics at Extreme Conditions, High Magnetic Field Laboratory, HFIPS, Chinese Academy of Sciences, Hefei, 230031, China*
[6]*College of Mathematics and Physics, Beijing University of Chemical Technology, Beijing 100029, China*
[7]*School of Physics and Physical Engineering, Qufu Normal University, Qufu 273165, China*
[8]*Institute for Theoretical Physics, University Hamburg, Jungiusstrasse 9, D-20355 Hamburg, Germany*
[9]*Theoretical Physics and Applied Mathematics Department, Ural Federal University, Mira Street 19, 620002 Ekaterinburg, Russia*
[10]*Institute for Molecules and Materials, Radboud University, Heijendaalseweg 135, NL-6525AJ Nijmegen, The Netherlands*
[11]*Collaborative Innovation Center of Microstructures, Nanjing University, Nanjing, 210093, China*

The nodal-line semimetals have attracted immense interest due to the unique electronic structures such as the linear dispersion and the vanishing density of states as the Fermi energy approaching the nodes. Here, we report temperature-dependent transport and scanning tunneling microscopy(spectroscopy)[STM(S)] measurements on nodal-line semimetal ZrSiSe. Our experimental results and theoretical analyses consistently demonstrate that the temperature induces Lifshitz transitions at 80 K and 106 K in ZrSiSe, which results in the transport anomalies at the same temperatures. More strikingly, we observe a V-shape dip structure around Fermi energy from the STS spectrum at low temperature, which can be attributed to co-effect of the spin-orbit coupling and excitonic instability. Our observations indicate the correlation interaction may play an important role in ZrSiSe, which owns the quasi-two-dimensional electronic structures.

Lifshitz transition, which is characterized by the change of the Fermi surface topology[1], can happen among various materials through changing some external parameters such as chemical doping, pressure or magnetic field[2–7]. Recently, a new type of temperature-driven Lifshitz transition has been observed in Dirac and Weyl semimetals, in which the transition usually happens as the Fermi energy crosses the Dirac and Weyl nodes[8–10]. Near these nodes, the carriers have high mobility and can switch from $n(p)$-type to $p(n)$-type as the Fermi energy decreases (increases) to cross the nodes[10]. As a consequence, a Lifshitz transition usually has a close relationship with the transport anomalies at low temperature in Dirac and Weyl semimetals[11–14]. However, no such transition has been observed in nodal-line semimetal. In terms of materials, the experimentally confirmed compounds include $PbTaSe_2$, $PtSn_4$ and ZrSiM (M=S, Se Te) family[15–21]. Among them, ZrSiM attracts much attention due to the quite large energy window of the linear band dispersion in some region of the Brillouin zone. As the element M changes from S to Te, the electronic structures between ZrSiM show some subtle but important differences. In ZrSiSe and ZrSiTe, some new tiny trivial bands could cross the Fermi energy. This feature implies the electronic structures of these two compounds are in the vicinity of a Lifshitz transition, which could be achieved by tuning some external parameters, such as temperature. Furthermore, the first-principles calculations predict a spin-orbit coupling (SOC) gap (20∼60 meV), which can destroy the nodal-line structure[15, 18, 21]. When the correlation interaction is taken into account, the nodal-line structure can further become instable and various correlation-driven nodal-line instabilities could emerge such as mass enhanced effect, excitonic insulator, charge/spin density wave etc[22–24]. These destructive instabilities could break down and obscure the topological physics based on the nodal-line structures in ZrSiM. However, the experimentally testing and verifying the destructive instabilities is still lacking.

In this work, we synthesize the high-quality single crystal ZrSiSe, and perform the detailed transport and scanning tunneling microscopy(spectroscopy) [STM(S)] measurements. The technical details are present in Supplemental Materials (SMs)[25]. The transport measurements show that ZrSiSe is a p-type metal above a critical temperature T= 106 K, whereas a portion of n-type carriers suddenly arise accompanying with the mobility sharply dropping when the temperature decreases below 106 K. As temperature further decreases, the mobility of n-type carriers suddenly ascends at another critical temperature T=80 K. In combined with the first-

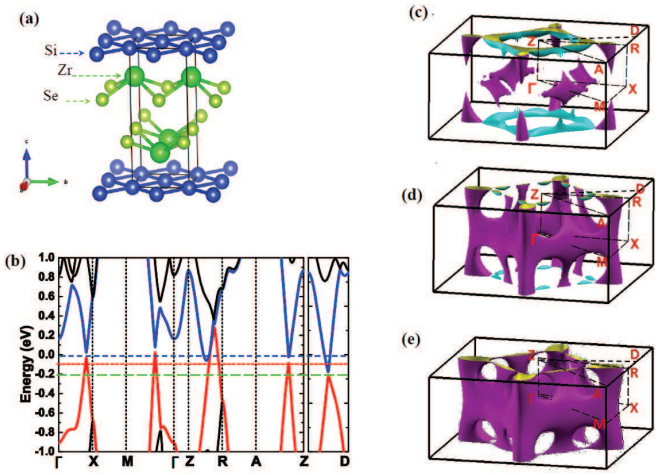

FIG. 1: (a) Crystal structure of ZrSiSe. (b) The first-principles calculated band structure of ZrSiSe with SOC along high-symmetry lines. The dashed blue line, dotted red and long dashed green lines label three different Fermi levels corresponding to the cases with temperature T=5 K (intrinsic case), 102 K and 106 K according to Fig. 2 (e), respectively. (c), (d) and (e) The three-dimensional Fermi surface with the Fermi energy labeled by the dashed blue, dotted red and long dashed green lines in (b), respectively.

principles calculations, these transport anomalies can be interpreted by the change of the topology of the Fermi surface induced by Fermi level shift as temperature changes. Furthermore, our STM/S measurements demonstrate the carrier density ratio between n-type and p-type develops from 0.7 at T=77 K to 0.95 at T=4.5 K. The charge neutrality from imbalance to balance as temperature decreases further proves the change of the topology of the Fermi surface. These self-consistent interpretations to the independent transport and STM/S measurements strongly indicate the temperature-dependent Lifshitz transition in ZrSiSe. Through investigating the average differential conductance spectra from STS measurements, we observe a V-shape dip structure around Fermi energy. Our theoretical model and analyses indicate that the dip formation in ZrSiSe is referable to the co-effect of SOC and the destructive correlation effect, which gives rise to the excitonic instability. Thus, ZrSiSe is a promising candidate for studying the destructive effect from correlation effect and SOC to Dirac nodal-line physics.

The crystal structure of ZrSiSe is shown in Fig. 1(a). ZrSiSe has a PbFCl-type crystal structure with space group $P4/nmm$. The band structure along some momentum lines are plotted in Fig. 1(b). When the Fermi level is at 0 eV (intrinsic case) in Fig. 1(b), a series of Dirac-type bands with linear dispersion form the nodal-line structure in the (k_x, k_y)-plane around k_z=0, which is similar to the bands in ZrSiS[22–24]. As k_z approaching π, however, along Z-R line, a new Fermi surface emerges as the band across the Fermi energy as shown in Fig. 1 (b).

Figure 2 (a) and (b) display representative ρ_{yx}-H and ρ_{xx}-H curves at selected temperatures. Detailed information is given in SMs[25]. As seen in Fig. 2(a), the $\rho_{yx}(H)$ curves exhibit three remarkable features. First, the nonlinearity for $\rho_{yx}(H)$ develops as the temperature decreases at low magnetic field. This feature indicates the carriers from multiband are involved in the transport as temperature decreases[12, 14]. Second, the $\rho_{yx}(H)$ curves have positive slope for $T>$ 40 K, which indicates the majority of carries are p-type at high temperature. Third, for $T<$ 40 K, the initial positive slope of $\rho_{yx}(H)$ curves tends to change sign as H increases from 0 T to 9 T, which indicates the compensated semimetal behavior with balance of n-type and p-type carriers at low temperature[12, 14]. In Fig. S2, temperature-dependent Hall coefficient, $R_H(T) = d\rho_{yx}(T)/dH$ at zero field limit shows a hump structure at T ∼106 K, which indicates the minimum value of the total carrier density as temperature crosses 106 K[25]. To further verifying the deductions, we analyze the Hall conductivity σ_{xy}=$\rho_{yx}/(\rho_{yx}^2+\rho_{xx}^2)$ and use the two-component model to extract the intrinsic carrier densities and carrier mobilities at various temperatures[9, 24].

$$\sigma_{xy} = (\frac{n_1\mu_1^2}{1+u_1^2B^2} + \frac{n_2\mu_2^2}{1+u_2^2B^2})eB. \quad (1)$$

Here, $n_1(n_2)$, $\mu_1(\mu_2)$ denote the carrier density [negative(positive)for electrons(hole)] and relevant in-plane mobility, respectively. In Fig. 2(c) and (d), the open symbols and the solid lines label the experiment data and the fitting results, respectively. The model fits well for the experimental data at all fixed temperatures. Figure 2 (e) and (f) show the temperature-dependent fitting parameters. At the lowest temperature T= 5 K, the magnitude of n_1 and n_2 is nearly balanced. As temperature increases, n_1 and μ_1 decrease smoothly. In contrast, μ_2 shows two sharp jumps at T=80 K and 106 K labeled by the left dashed red and right dashed green lines in Fig. 2 (f), respectively. n_2 sharply decreases and becomes positive above T=106 K with negligible value in comparison with n_1.

Now, we elaborate the temperature-induced Lifshitz transition can give a natural interpretation to these transport anomalies. The Hall analyses in Fig. 2 clarify that the compensated electrons and holes at low temperature and the majority of p-type carriers at high temperature. In combined with Fig. 1, these behaviors imply that ZrSiSe should have zero Fermi level E_F=0 eV at low temperature and the Fermi level should descend at high temperature. Such Fermi level shift driven by temperature can be induced by the change of the lattice constants [10] supported by our powder X-ray diffraction (XRD) measurements (See Fig. S6 and Fig. S7 in SMs for details)[25], the localization or delocalization induced by

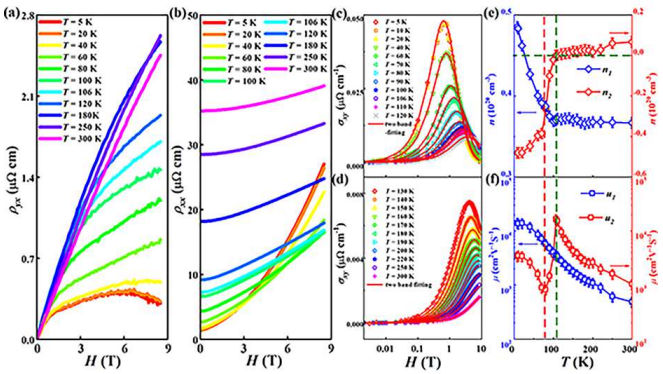

FIG. 2: (a)-(b) The field dependence of the $\rho_{yx}(H)$ and $\rho_{xx}(H)$ for several temperatures ranging from T= 5 K to 300 K. (c)-(d) The field dependence of the Hall conductivity $\sigma_{xy}(H)$ for temperatures ranging from T= 5 K to 300 K. Open symbols represent the experimental results and the red solid lines represent the fitting results based on two-component model. (e)-(f) The temperature dependence of fitting parameter, namely, the densities and mobility of the carriers extracted from the two-component model analysis of σ_{xy}. The left dashed red and right dashed green lines in (f) label two anomalies of the mobility μ_2 at 80 K and 106 K respectively.

the unavoided impurities and the thermal phonons[38], and the band renormalization[39] induced by electron-phonon coupling via self-energy effect. From Fig. 1 (b) and (c), p-type (n_1 , μ_1) component can be identified to the magenta Fermi pockets from the red band while the n-type (n_2 , μ_2) component corresponds to the cyan Fermi pockets from the blue band at T=5 K. As temperature increase, the first jump of μ_2 emerges at T=80 K. This can be understood by the band characteristics below and above 80 K. Below 80 K, such as 5 K as shown in Fig. 1(c), the n-type cyan Fermi pockets include both low-mobility carriers with quadratic dispersion (Z-R line in Fig. 1(b)) and high-mobility carriers with linear dispersion (Z-D line in Fig. 1(b)). Above 80 K, such as 102 K as shown in Fig. 1(d), the n-type cyan Fermi pockets only include high-mobility carriers with linear dispersion (Z-D line in Fig. 1(b)). It indicates that 80 K must correspond to the Fermi level crossing the quadratic band bottom along the Z-R line in Fig.1 (b). Meanwhile, n-type cyan Fermi pocket splits from one to eight, which indicates a Lifshitz transition happens at 80 K. As temperature further increases, the second jump of μ_2 emerges at T=106 K. μ_2 reaches a maximal value from 102 K to 106 K. This process corresponds to shifting the Fermi level from the position labeled by the dotted red line to the Dirac point labeled by the long dashed green line in Fig. 1(b), because the carriers at Dirac point have the largest mobility. Above 106 K, the Fermi level descends below the Dirac point. The n-type Fermi pockets disappear (the blue band is not occupied in Fig. 1(b)), and only the p-type Fermi pockets survive (only the red band is occupied in Fig. 1(b)). It means that the n-type component (n_2 , μ_2) undergoes the second Lifshitz transition at 106 K. Note that it seems that two p-type components still exist from Fig. 2(e) and (f), though only one band survives. In the whole temperature regime, two-component model is adopted to fit the experimental results. It is natural for each component is not zero. However, above 106 K, the weight of one component should be very small. It is explicit that n_2 is insignificantly small in comparison to n_1. Meanwhile, the μ_1 and μ_2 have the same trend. Thus, above 106 K, we argue that the n_1 and n_2 may be from the same band (red band in Fig. 1 (b)), and the small value of n_2 may be from the anisotropy of the magenta Fermi pockets in Fig. 1(e).

STM/S can help to understand the picture extracted from and or beyond the transport measurements[40–45]. Figure 3 (b) shows the topography of a Se cleaved surface and the corresponding fast Fourier transform (FFT) image at T= 4.5 K. Figure 3 (c) and (d) show the zoom-in view of the topography at T= 4.5 K and T= 77 K, in which the two interleaved lattices (Zr and Se) and the Si square net can be well identified. We next presented in the Fig. 3 (e) and Fig. S9 the line-cut averaged dI/dV spectra (proportional to the density of states (DOS)) measured at T= 4.5 K (black curve) and T= 77 K (red curve) along different scanning paths. The spectra in Fig.3 (e) and Fig. S9 are averaged by taking several spectra along a Zr-Se-Zr line, and Se-Si-Se line, respectively. The remarkable difference between two spectrum appears at near zero bias. A broad V-shape dip emerges at T= 4.5 K and disappears at T= 77 K. To estimate the temperature-driven change of carriers density, we present the line-cut map crossing four unit cells (UCs) along Zr-Se-Zr line at T= 4.5 K in Fig. 3 (f). The original dI/dV spectra were shown in Fig. S8 in SMs[25]. The position-dependent STS spectrum[46] and angle-resolved photoemission spectroscopy[15, 21] have proven that Zr and Se in ZrSiSe dominate the holes channel and electron channel, respectively, which is similar with some semiconductor materials, such as GaAs[47]. Thus, the imbalance between electron extraction at negative bias and electron injection at positive bias, *i.e.*, the ratio of e-h asymmetric $R(r)$, could be directly obtained through the following equation[43–45],

$$R(r) = \frac{\int_{E_F}^{-E_1} N(r,E)\,dE}{\int_{E_2}^{E_F} N(r,E)\,dE}. \qquad (2)$$

By integrating the filled and empty states in the vicinity of the E_F from -100 mV to 100 mV, the result was shown in Fig. 3g. The e/h ratio varies between 0.88 and 1.02 within a unit cell, while the overall ratio takes the value e/h=0.95, indicating the nearly perfect compensated band structure. At T= 77 K, as shown in Fig. 3(h) and (i), the orbital texture changes obviously comparing

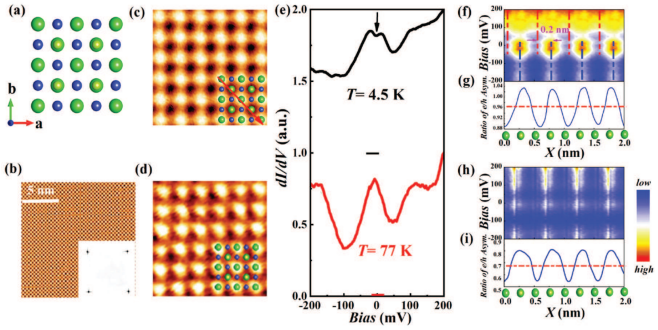

FIG. 3: (a)Top view of crystal structure of ZrSiSe. (b) Atomically resolved STM topographic image of the cleaved ZrSiSe surface at T= 4.5 K with V_b = 600 mV and I_t= 200 pA. The inset shows the fast Fourier transform (FFT) image. (c)-(d) Zoom-in views of the cleaved surface at T= 4.5 K (V_b= 600 mV and I_t= 500 pA) and T= 77 K (V_b= 600 mV and I_t= 200 pA). (e) Line-cut averaged dI/dV spectrum acquired in ZrSiSe at T= 4.5 K (black curve) and T= 77 K (red curve) along the Zr-Se-Zr direction. All spectra are normalized at V=200 mV. The black-solid arrow labels the V-shape dip structure. The red-solid arrow in Fig.3(c) labels the line-cut direction. (f) and (h) The STS line-cut map along the Zr-Se-Zr direction at T= 4.5 K and 77 K, respectively. (g) and (i) The calculated ratio of e/h asymmetry based on the spectra measurement in (f) and (h), respectively.

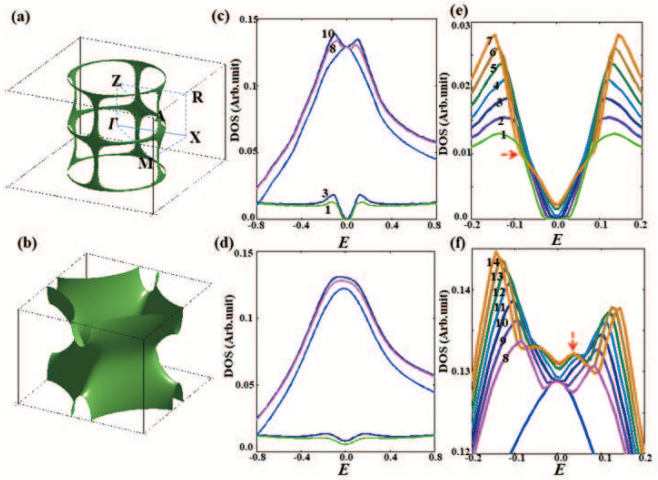

FIG. 4: (a) and (b)The calculated Dirac nodal-line structure and Fermi surface of trivial quadratic band with the model in SMs, respectively. (c) and (d) The calculated DOS with the model in SMs for k_BT=0.004 (T= 4.5 K) in (c) and k_BT=0.05 (T=77 K) in (d). Bottom curve 1 and 3 are from Dirac nodal-line bands in (a) with (λ_{soc}, Δ_{ex})=(0.06, 0) and (0.06, 0.02), respectively. Top curve 8 and 10 are from the sum of blue curve and bottom curves 1 and 3, respectively. (e) and (f) The zoom-in of the bottom and top parts of (c), respectively. Curves 1 and 3 in (e) and (f) are same to these in (c). The curves 2, 4-7 with (λ_{soc}, Δ_{ex})=(0.06, 0.01), (0.06, 0.03-0.06). The curves 9, 11-14 have the same values as the curves 2, 4-7. In (a)-(f), other parameters are present in SMs.

with the case at T= 4.5 K. The overall e/h ratio equals 0.7. Note that the choice of integration limits [-100 meV, 100 meV] guarantees that evolution of the n-type band is smooth and undergoes a Lifshifz transition from the Fermi levels of 4.5 K and 77 K to -100 meV, respectively. In comparison with the calculated results shown in Fig. 1 (b), (c), (d) and the two-component model fitting results shown in Fig. 2 (e), the temperature-induced carriers density evolution obtained from STM/S measurement follows the same tendency and supports the temperature induced Lifshifz transitions. The banlanced e/h ratio also provides a straightforward explanation of the non-saturated magnetoresistance (MR) at T=5 K (See Fig. S10 for details)[25, 48, 49].

Now, we turn to understand the V-shape dip of dI/dV at temperature T= 4.5 K. Besides SOC, there exists several possible mechanism to induce the V-shape dip. Since our sample is very clean with the mobility as high as $10^4 cm^2 V^{-1} S^{-1}$, which excludes the possible disorder effect, such as the well-known zero-bias anomaly[50–57]. The correlated interaction can induce some long-range order, such as superconducting and excitonic orders. The superconducting order can be easily excluded, because the V-shape dip structure is robust against the strong magnetic field in our measurement. Recall that a quite strong Coulomb interaction can open an excitonic gap to the Dirac nodes in two-dimensional graphene and the mass enhancement has been recently observed in ZrSiS[58–61]. It is naturally to think that the Dirac nodal-line structure can be gapped by the similar excitonic order, which results in the V-shape dip. To verify such a deduction and figure out the relation between SOC, excitonic instability and the V-shape dip structure. We construct a simplified model to do a simulation. Let's reconsider the Hall analyses in Fig. 2 and the electronic structure in Fig. 1 (b) and (c). The minimal model should includes two parts at least. One part captures the Dirac nodal-line bands, while another part describes the trivial quadratic band. Note that the effect of surface bands can merge into the trivial quadratic band, because surface bands only contribute a large trivial electron pockets centered at M point and four small hole pockets around X point in surface Brillouin zone[62, 63]. Furthermore, both bulk DOS and surface DOS are calculated (See Fig. S3 in SMs for details)[25]. Without considering the excitonic instability, none of them can produce the V-shape dip feature.

The detailed theoretical modeling is presented in the SMs[25], and we only list the results here. Figure 4(a) and (b) simulates Dirac nodal-line structure and Fermi surface from the trivial quadratic band. Figure 4 (c) gives several calculated DOS curves with different SOC λ_{soc} and excitonic order parameter Δ_{ex}. The curve 1 indicates nonzero λ_{soc} can open a gap to the Dirac nodal lines. The

curve 3 indicates the coexistence of both λ_{soc} and Δ_{ex} can suppress the nodal-line gap opened by λ_{soc}. The blue color curve gives the DOS of the trivial quadratic band from Fig. 4 (b). The curve 8 is the sum from the curve 1 and the blue color one, which is not similar to the 4.5 K experimental result shown in Fig. 3 (e). It indicates that the sole SOC λ_{soc} can not explain the experimental result. However, by taking into account both SOC λ_{soc} and the excitonic order parameter Δ_{ex}, the cure 10 give similar result in Fig. 3 (e) at 4.5 K. Furthermore, The thermal broadening effect of dI/dV is proportional to $\int d\omega[-f'(\omega - eV)N(\omega)]$ with f and $N(\omega)$ the Fermi function and zero-temperature DOS, respectively. The missing V-shape dip structure of the dI/dV curve at 77 K shown in Fig. 3 (e) is well captured by Fig. 4 (d). To see the effect of both λ_{soc} and Δ_{ex} clearer, the zoom-in parts of Fig.4 (c) are shown in Fig. 4 (e) and (f), where more curves with different values of Δ_{ex} are plotted besides the ones in Fig. 4 (c). As Δ_{ex} increases from zero, the curves 5, 6, 7 show the visible two dip structures labeled by the red-dashed arrow in Fig. 4 (e). Then, the dip structures of relevant curves 12, 13, 14 become to deviate from the V-shape labeled by the red-dashed arrow in Fig. 4 (f). According to our simulation, the optimal value of Δ_{ex} to obtain the V-shape dip structure is $\Delta_{ex} \sim 1/3\lambda_{soc}$, which can strongly suppress the SOC gap without induce visible two-dip structure.

In conclusion, our transport, STM/S measurements and theoretical analyses consistently demonstrate that the temperature induces Lifshitz transitions in ZrSiSe. We also observed a V-shape dip structure around Fermi energy from the STS spectrum at low temperature. Our theoretical modeling simulation clarifies the V-shape dip structure is from the co-effect of SOC and possible excitonic instability. Our observations indicate correlation interaction in ZrSiSe deserves to attract more attention in the future studies.

Acknowledgements-This work was supported by the National Key R&D Program (2016YFA0300404, 2016YFA0401803, 2017YFA0303201, 2015CB921103, 2019YFA0308602), the National Nature Science Foundation of China (11674326, 11674331, 11774351, 11874357, 11625415, 11374260, U1432139, U1832141, U1932217), Key Research Program of Frontier Sciences, CAS (QYZDB-SSW-SLH015), the "Strategic Priority Research Program (B)" of the Chinese Academy of Sciences, Grant No. XDB33030100, the '100 Talents Project' of the Chinese Academy of Sciences, CASHIPS Director's Fund (No. BJPY2019B03) and Science Challenge Project (No. TZ2016001). A portion of this work was supported by the High Magnetic Field Laboratory of Anhui Province, the Fundamental Research Funds for the Central Universities in China, the European Research Council under the European Union's Seventh Framework Program (FP/2007-2013) through ERC Grant No. 338957 and by NWO via Spinoza Prize, and the Cluster of Excellence "The Hamburg Centre for Ultrafast Imaging (CUI)' of the German Science Foundation (DFG).

* These authors have contributed equally to this work.
† Electronic address: xluo@issp.ac.cn
‡ Electronic address: yiyin@zju.edu.cn
§ Electronic address: haon@hmfl.ac.cn
¶ Electronic address: ypsun@issp.ac.cn

[1] I. M. Lifshitz, Sov. Phys. JETP **11**, 1130-1135 (1960).
[2] Y. Okada, M. Serbyn, H. Lin, D. Walkup, W. Zhou, C. Dhital, M. Neupane, S. Xu, Y. Wang, R. Sankar, F. Chou, A. Bansil, M. Z. Hasan, S. D. Wilson, L. Fu and V. Madhavan, Science **341**, 1496-1499 (2013).
[3] C. Liu, T. Kondo, R. M. Fernandes, A. Palczewski, E. D. Mun, N. Ni, A. N. Thaler, A. Bostwick, E. Rotenberg, J. Schmalian, S. L. Bud'ko, P. C. Canfield and A. Kaminski, Nat. Phys. **6**, 419-423 (2010).
[4] Z. J. Xiang, G. J. Ye, C. Shang, B. Lei, N. Z. Wang, K. S. Yang, D. Y. Liu, F. B. Meng, X. G. Luo, L. J. Zou, Z. Sun, Y. Zhang and X. H. Chen, Phys. Rev. Lett. **115**, 186403 (2015).
[5] L. J. Zhang, C. Y. Guo, X. D.Zhu, L. Ma, G. L. Zheng, Y. Q. Wang, L. Pi, Y. Chen, H. Q. Yuan and M. L. Tian, Phys. Rev. Lett. **118** , 206601 (2017).
[6] D. Aoki, G. Seyfarth, A. Pourret, A. Gourgout, A. McCollam, J. A. N. Bruin, Y. Krupko and I. Sheikin, Phys. Rev. Lett. **116**, 037202 (2016).
[7] G. Bastien, A. Gourgout, D. Aoki, A. Pourret, I. Sheikin, G. Seyfarth, J. Flouquet and G. Knebel, Phys. Rev. Lett. **117**, 206401 (2016).
[8] Y. Wu, N. H. Jo, M. Ochi, L. Huang, D. Mou, S. L. Bud'ko, P. C. Canfield, N. Trivedi, R. Arita and A. Kaminski, Phys. Rev. Lett. **115**, 166602 (2015).
[9] F. C. Chen, H. Y. Lv, X. Luo, W. J. Lu, Q. L. Pei, G. T. Lin, Y. Y. Han, X. B. Zhu, W. H. Song and Y. P. Sun, Phys. Rev. B **94**, 235154 (2016).
[10] Y. Zhang, C. Wang, L. Yu, G. Liu, A. Liang, J. Huang, S. Nie, X. Sun, Y. Zhang, B. Shen, J. Liu, H. Weng, L. Zhao, G. Chen, X. Jia, C. Hu, Y. Ding, W. Zhao, Q. Gao, C. Li, S. He, L. Zhao, F. Zhang, S. Zhang, F. Yang, Z. Wang, Q. Peng, X. Dai, Z. Fang, Z. Xu, C. Chen and X. J. Zhou, Nat. Commun. **8**, 15512 (2017).
[11] H. Weng, X. Dai and Z. Fang, Phys. Rev. X **4**, 011002 (2014).
[12] K. Akiba, A. Miyake, Y. Akahama, K. Matsubayashi, Y. Uwatoko and M. Tokunaga, Phys. Rev. B **95**, 115126 (2017).
[13] G. Manzoni, A. Sterzi, A. Crepaldi, M. Diego, F. Cilento, M. Zacchigna, Ph. Bugnon, H. Berger, A. Magrez, M. Grioni and F. Parmigiani, Phys. Rev. Lett. **115**, 207402 (2015).
[14] H. Chi, C. Zhang, G. Gu, D. E. Kharzeev, X. Dai and Q. Li, New J. Phys. **19**, 015005 (2017).
[15] Q. Xu, Z. Song, S. Nie, H. Weng, Z. Fang and X. Dai, Phys. Rev. B **92**, 205310 (2015).
[16] Y. Wu, L. Wang, E. Mun, D. D. Johnson, D. Mou, L. Huang, Y. Lee, S. L. Bud'ko, P. C. Canfield and A. Kaminski, Nat. Phys. **12**, 667-671 (2016).
[17] G. Bian, T. R. Chang, R. Sankar, S. Xu, Ha. Zheng, T. Neupert, C. Chiu, S. Huang, G. Chang, I. Belopolski, D.

S. Sanchez, M. Neupane, N. Alidoust, C. Liu, B. Wang, C. Lee, H. Jeng, C. Zhang, Z. Yuan, S. Jia, A. Bansil, F. Chou, H. Lin and M. Z. Hasan, Nat. Commun. **7**, 10556 (2016).

[18] L. M. Schoop, M. N. Ali, C. Straßer, A. Topp, A. Varykhalov, D. Marchenko, V. Duppel, S. S. P. Parkin, B. V. Lotsch and C. R. Ast, Nat. Commun. **7**, 11696 (2016).

[19] M. N. Ali, L. M. Schoop, C. Garg, J. M. Lippmann, E. Lara, B. Lotsch and S. S. P. Parkin, Sci. Adv. **2**, e1601742 (2016).

[20] J. Hu, Z. Tang, J. Liu, X. Liu, Y. Zhu, D. Graf, K. Myhro, S. Tran, C. N. Lau, J. Wei and Z. Mao, Phys. Rev. Lett. **117**, 016602 (2016).

[21] M. M. Hosen, K. Dimitri, I. Belopolski, P. Maldonado, R. Sankar, N. Dhakal, G. Dhakal, T. Cole, P. M. Oppeneer, D. Kaczorowski, F. Chou, M. Z. Hasan, T. Durakiewicz and M. Neupane, Phys. Rev. B **95**, 161101 (2017).

[22] Y. Huh, E. Moon and Y. B. Kim, Phys. Rev. B **93**, 035138 (2016).

[23] J. Liu and L. Balents, Phys. Rev. B **95**, 075426 (2017).

[24] B. Roy, Phys. Rev. B **96**, 041113 (2017).

[25] See Supplemental Material at [url] for details on the sample preparation, sample characterization, band structure calculations and the theoretical modeling of the STS spectra,which includes Refs. [19, 26 – 37].

[26] P. Hohenberg and W. Kohn, Phys. Rev. **136**, B864 (1964).

[27] W. Kohn and L. J. Sham, Phys. Rev. **140**, A1133 (1965).

[28] G. Kresse and J. Hafner, Phys. Rev. B **49**, 14251 (1994).

[29] G. Kresse and J. Furthmüller, Comput. Mater. Sci. **6**, 15 (1996).

[30] G. Kresse and J. Furthmüller, Phys. Rev. B **54**, 11169 (1996).

[31] John P. Perdew, Kieron Burke, and Matthias Ernzerhof. Phys. Rev. Lett. **77**, 3865 (1996).

[32] P. E. Blöchl, Phys. Rev. B **50**, 17953 (1994).

[33] G. Kresse and D. Joubert, Phys. Rev. B **59**, 1758 (1999).

[34] C. Wang and T. Hughbanks, Inorg. Chem. **34**, 5524 (1995).

[35] F. F. Tafti, Q. D. Gibson, S. K. Kushwaha, N. Haldolaarachdhige and R. J. Cava, Nat. Phys. **12**, 272-277, (2015).

[36] F. F. Tafti, Q. D. Gibson, S. K. Kushwaha, J. W. Krizan, N. Haldolaarachdhige and R. J. Cava, Proc. Natl. Acad. Sci. USA **113**, E3475-3481, (2016).

[37] X. Luo, F. C. Chen, Q. L. Pei, J. J. Gao, J. Yan, W. J. Lu, P. Tong, Y. Y. Han, W. H. Song and Y. P. Sun, Appl. Phys. Lett. **110**, 092401, (2017).

[38] D. N. McIlroy, S. Moore, D. Zhang, J. Wharton, B. Kempton, R. Littleton, M. Wilson, T. M. Tritt and C. G. Olson, J. Phys.: Condens. Matter. **16**, L359-356 (2004).

[39] Y. S. Kushnirenko, A. A. Kordyuk, A. V. Fedorov, E. Haubold, T. Wolf, B. Büchner, and S. V. Borisenko Phys. Rev. B **96**, 100504(R) (2017).

[40] A. Piriou, N. Jenkins, C. Berthod, I. M. Aprile and ∅. Fischer, Nat. Commun. **2**, 221 (2011).

[41] S. Qiao, X. Li, N. Wang, W. Ruan, C. Ye, P. Cai, Z. Hao, H. Yao, X. Chen, J. Wu, Y. Wang and Z. Liu, Phys. Rev. X **7**, 041054 (2017).

[42] R. Wu, J. Z. Ma, S. M. Nie, L. X. Zhao, X. Huang, J. X. Yin, B. B. Fu, P. Richard, G. F. Chen, Z. Fang, X. Dai, H. M. Weng, T. Qian, H. Ding, and S. H. Pan, Phys. Rev. X **6**, 021017 (2016).

[43] Y. Kohsaka, C. Taylor, K. Fujita, A. Schmidt, C. Lupien, T. Hanaguri, M. Azuma, M. Takano, H. Eisaki, H. Takagi, S. Uchida, J. C. Davis, Science **315**, 1380-1385 (2007).

[44] M. Randeria, R. Sensarma, N. Trivedi and F. C. Zhang, Phys. Rev. Lett. **95**, 137001 (2005).

[45] B. Phillabaum, E. W. Carlson and K. A. Dahmen, Nat. Commun. **3**, 915 (2012).

[46] K. Bu, Y. Fei, W. Zhang, Y. Zheng, J. Wu, F. Chen, X. Luo, Y. P. Sun, Q. Xu, X. Dai and Yi Yin, Phys. Rev. B **98**, 115127 (2018).

[47] R. M. Feenstra, J. A. Stroscio, J. Tersoff and A. P. Fein, Phys. Rev. Lett. **58**, 1192 (1987).

[48] C. Shekhar, A. K. Nayak, Y. Sun, M. Schmidt, M. Nicklas, I. Leermakers, U. Zeitler, Y. Skourski, J. Wosnitza, Z. Liu, Y. Chen, W. Schnelle, H. Borrmann, Y. Grin, C. Felser and B. Yan, Nat. Phys. **11**, 645 (2015).

[49] M. N. Ali, J. Xiong, S. Flynn, J. Tao, Q. D. Gibson, L. M. Schoop, T. Liang, N. Haldolaarachchige, M. Hirschberger, N. P. Ong and R. J. Cava, Nature **514**, 205 (2014).

[50] F. G. Pikus and A. L. Efros, Phys. Rev. B **51**, 16871-16877 (1995).

[51] A. L. Efros, B. Skinner and B. I. Shklovskii, Phys. Rev. B **84**, 064204 (2011).

[52] A. L. Efros, Phys. Rev. Lett. **68**, 2208 (1992).

[53] J. G. Massey and M. Lee, Phys. Rev. Lett. **75**, 4226 (1995).

[54] B. L. Altshuler, A. G. Aronov and P. A. Lee, Phys. Rev. Lett. **44**, 1288 (1980).

[55] J. P. Eisenstein, L. N. Pfeiffer and K. N. West, Phys. Rev. Lett. **69**, 3804 (1992).

[56] Z. Y. Jia, Y. H. Song, X. B. Li, K. Ran, P. Lu, H. J. Zheng, X. Y. Zhu, Z. Q. Shi, J. Sun, J. S. Wen, D. Y. Xing and S. C. Li, Phys. Rev. B **96**, 041108 (2017).

[57] Y. H. Song, Z. Y. Jia, D. Zhang, X. Y. Zhu, Z. Q. Shi, H. Wang, L. Zhu, Q. Q. Yuan, H. Zhang, D. Y. Xing and S. C. Li, Nat. Commun **9**, 4071 (2018).

[58] V. N. Kotov, B. Uchoa, V. M. Pereira, F. Guinea and A. H. Castro Neto, Rev. Mod. Phys. **84**, 1067 (2012).

[59] A. N. Rudenko, E. A. Stepanov, A. I. Lichtenstein and M. I. Katsnelson Phys. Rev. Lett. **120**, 216401 (2018).

[60] M. M. Scherer, C. Honerkamp, A. N. Rudenko, E. A. Stepanov, A. I. Lichtenstein and M. I. Katsnelson, Phys. Rev. B **98**, 241112 (2018).

[61] S. Pezzini, M. R. van Delft, L. M. Schoop, B. V. Lotsch, A. Carrington, M. I. Katsnelson, N. E. Hussey and S. Wiedmann, Nat. Phys. **14**, 178 (2018).

[62] A. Topp, R. Queiroz, A. Grüneis, L. Müchler, A. W. Rost, A. Varykhalov, D. Marchenko, M. Krivenkov, F. Rodolakis, J. L. McChesney, B. V. Lotsch, L. M. Schoop and C. R. Ast, Phys. Rev. X **7**, 041073 (2017).

[63] B. B. Fu, C. J. Yi, T. T. Zhang, M. Caputo, J. Z. Ma, X. Gao, B. Q. Lv, L. Y. Kong, Y. B. Huang, P. Richard, M. Shi, V. N. Strocov, C. Fang, H. M. Weng, Y. G. Shi, T. Qian and H. Ding, Sci. Adv. **5**, eaau6459 (2019).